

MIXED HIGGS-RADION STATES AT THE LHC – A DETAILED STUDY

Amit Chakraborty¹Theory Center, Institute of Particle and Nuclear Studies,
KEK, 1-1 Oho, Tsukuba, Ibaraki 305-0801, JapanUshoshi Maitra², Sreerup Raychaudhuri³ and Tousik Samui⁴Department of Theoretical Physics, Tata Institute of Fundamental Research,
1, Homi Bhabha Road, Mumbai 400 005, India.

October 27, 2021

ABSTRACT

Light radions constitute one of the few surviving possibilities for observable new particle states at the sub-TeV level which arise in models with extra spacetime dimensions. It is already known that the 125 GeV state discovered at CERN is unlikely to be a pure radion state, since its decays resemble those of the Standard Model Higgs boson too closely. However, due to experimental errors in the measured decay widths, the possibility still remains that it could be a mixture of the radion with one (or more) Higgs states. We use the existing LHC data at 8 and 13 TeV to make a thorough investigation of this possibility. Not surprisingly, it turns out that this model is already constrained quite effectively by direct LHC searches for an additional scalar heavier than 125 GeV. We then make a detailed study of the so-called ‘conformal point’, where this heavy state practically decouples from (most of) the Standard Model fields. Some projections for the future are also included.

PACS Nos: 04.60.Bc, 12.60.Fr, 14.80.Cp, 13.85.Rm

1. INTRODUCTION

The 2012 discovery [1], at the LHC, of a weakly-interacting light scalar state — which appears from all current indications to be an elementary Higgs particle — revives the old question of how the mass of such a scalar can remain stable against large electroweak corrections in a theory with a momentum cutoff at some very high scale. This, as is well-known, goes by the name of the gauge hierarchy problem, or, alternatively, as the fine-tuning problem. It has also been known for several decades that any solution to this problem must invoke new physics beyond the Standard Model (SM) of strong and electroweak interactions.

¹E-mail: amit@post.kek.jp²E-mail: ushoshi@theory.tifr.res.in³E-mail: sreerup@theory.tifr.res.in⁴E-mail: tousik@theory.tifr.res.in

One of the most elegant solutions of the hierarchy problem is that devised in 1999 by L. Randall and R. Sundrum (RS) [2]. They considered a world with one extra space dimension, having the topology of a circle folded about a diameter ($\mathbb{S}^1/\mathbb{Z}_2$), at either end of which lies a pair of four-dimensional manifolds – called ‘branes’ – containing matter. One of these is the so-called infra-red (IR) brane, where all the SM fields lie, and the other is the so-called ultra-violet (UV) brane, where we have field elements comprising a theory of strong⁵ gravity. One can then tune the cosmological constant on the two branes, as well as that in the $\mathbb{S}^1/\mathbb{Z}_2$ bulk, to obtain a solution of the five-dimensional Einstein equations in the form of a ‘warped’ metric

$$ds^2 = e^{-2\mathcal{K}R_c\phi}\eta_{\mu\nu}dx^\mu dx^\nu - R_c^2 d\phi^2 \quad (1)$$

where the $\mathbb{S}^1/\mathbb{Z}_2$ ‘throat’ is characterised by the compactification radius R_c , an angular coordinate ϕ and a curvature parameter \mathcal{K} . It can then be shown that the mass of the Higgs scalar is generated on the UV brane at a value close to the bulk Planck mass M_5 (itself a little smaller than the four-dimensional Planck mass $M_P = (\hbar c/G_N)^{1/2}$), and projected on the IR brane through the expanding ‘throat’, thereby acquiring the much smaller value

$$M_H \sim e^{-\pi\mathcal{K}R_c} M_5 \quad (2)$$

If we can now tune $\mathcal{K}R_c \simeq 11.6$, we recover the correct ballpark for the mass of the discovered scalar. This constitutes a neat solution to the hierarchy problem in terms of spacetime geometry, without having recourse to any parameters which are unnaturally large or small. In fact, the Planck scale is the only fundamental mass scale in this theory.

It is fair to ask, however, whether the parameter $\mathcal{K}R_c$ is protected against small dynamical fluctuations, for

$$\frac{\delta M_H}{M_H} \approx 11.6\pi \frac{\delta R_c}{R_c} \quad (3)$$

i.e. small fluctuations in the inter-brane distance would lead to magnified fluctuations in the Higgs boson mass. As the latter is now known to an accuracy of about 2%, it follows that the inter-brane distance must be stable to an accuracy of about 5×10^{-4} — for which the minimal RS model has *no* provision.

A brilliant solution to this was devised by Goldberger and Wise (1999) [3]. If one allows for

⁵Here ‘strong’ means comparable to electroweak strength.

fluctuations in the size of the extra dimension, we can rewrite the metric in Eq. (1) as

$$ds^2 = e^{-2T(x)\phi} \eta_{\mu\nu} dx^\mu dx^\nu - \left[\frac{T(x)}{\mathcal{K}} \right]^2 d\phi^2 \quad (4)$$

where the dynamic $T(x)$ replacing $\mathcal{K}R_c$ is known as a modulus field. In the minimal RS model, this is a free field and hence, as mentioned above, there is no constraint at all on $\mathcal{K}R_c = \langle T(x) \rangle$. Goldberger and Wise then augmented the model by the introduction of a bulk scalar $B(x, y)$, with a mass M_B and quartic self-interactions on the IR and UV branes, with vacuum expectation values V_{IR} and V_{UV} respectively – all these mass-dimension quantities being in the ballpark of the Planck mass. They were then able to show that the scalar modulus field $T(x)$ develops a potential with a minimum at

$$\langle T(x) \rangle = \mathcal{K}R_c \simeq \frac{4}{\pi} \left(\frac{\mathcal{K}}{M_B} \right)^2 \ln \frac{V_{UV}}{V_{IR}} \quad (5)$$

which can be easily tuned to the required value 11.6 by varying the unknowns M_B , V_{IR} and V_{UV} without having recourse to unnaturally large or small numbers. This is consistent with the general philosophy of the RS model.

The modulus field $T(x)$, which is like a dilaton in the fifth dimension, can be parametrised as a *radion*

$$\varphi(x) = \Lambda_\varphi e^{-\pi\{T(x)-\mathcal{K}R_c\}} \quad (6)$$

which has a vacuum expectation value

$$\Lambda_\varphi = \sqrt{\frac{24M_5^3}{\mathcal{K}}} e^{-\pi\mathcal{K}R_c} \quad (7)$$

and a mass

$$M_\varphi^2 = \frac{2\mathcal{K}^2}{M_5^3} (V_{UV} - V_{IR})^2 e^{-2\pi\mathcal{K}R_c} \quad (8)$$

Because of the warp factor $e^{-\pi\mathcal{K}R_c}$, both the radion mass M_φ and the radion vacuum expectation value Λ_φ lie at or around the electroweak scale. Hence, it is easier, for phenomenological purposes, to treat them as the free parameters in the theory, rather than the set $\{\mathcal{K}, M_5, V_{UV}, V_{IR}\}$. It is also worth noting that if we let $V_{UV} = V_{IR}$, in which case Eq. (8) tells us that the radion is massless, we would also have $R_c = 0$ from Eq. (5), i.e. the two branes would coalesce and M_H immediately shoot up to M_5 — which takes us back to the Standard Model and the hierarchy problem. We conclude, therefore, that $V_{UV} > V_{IR}$ and hence the radion must be massive.

The interactions of the radion with matter on the IR brane will naturally follow those of the dilaton (which it is a variant of) and can be written as

$$\mathcal{L}_{\text{int}}(\varphi) = \frac{1}{\Lambda_\varphi} \varphi (T_\mu^\mu + \mathcal{A}_T) \quad (9)$$

where $T_{\mu\nu}$ is the tree-level energy-momentum tensor and \mathcal{A}_T is the trace anomaly. For on-shell particles, the tree-level T_μ^μ has the explicit form

$$T_\mu^\mu = \sum_f m_f \bar{f} f + M_H^2 H^2 - 2M_W^2 W^{+\mu} W_\mu^- - M_Z^2 Z^\mu Z_\mu \quad (10)$$

where the sum runs over all fermions f . This, apart from the \mathcal{A}_T term, is exactly like the coupling of the Higgs boson, except that the SM vacuum expectation value v is replaced by the radion vacuum expectation value Λ_φ . Not surprisingly, radion phenomenology is very similar to Higgs boson phenomenology. It differs, however, in the anomaly term

$$\mathcal{A}_T = \sum_i \frac{\beta(g_i)}{2g_i} F^{\mu\nu i} F_{\mu\nu}^i \quad (11)$$

where $\beta(g_i)$ is the beta function corresponding to the coupling g_i of the gauge field A_i which has the field strength tensor $F_{\mu\nu}^i$. The sum over i runs over all the gauge fields in the SM, including photons, gluons and W^\pm and Z bosons. The \mathcal{A}_T term induces substantial couplings of the radion to $\gamma\gamma$ and gg pairs, which are completely absent in Eq. (10). On the other hand, similar anomaly-induced contributions to radion couplings with W^+W^- and ZZ pairs are usually negligible compared to the corresponding terms in Eq. (10), because of the large masses of these particles, and only become significant when their tree-level couplings to one of the scalars vanishes.

Like the Higgs boson, the tree-level radion couplings in Eqn. (9) would be subject, in addition to the trace anomaly contributions, to radiative corrections, especially from loops involving the top quark. Moreover, it is worth mentioning that there could be large brane corrections to the above couplings if the mass of the radion is comparable to the Kaluza-Klein scale [4], determined by the mass of the lightest graviton mode in the minimal RS construction. To avoid this, we require a radion which is comparatively light, and this requires a modest level of fine tuning [4]. The discussions in this article are, therefore, subject to this assumption.

As remarked above, the phenomenological behaviour of such a light radion is rather similar to that of the Higgs boson. This naturally leads one to ask whether these two low-lying

elementary scalar states can *mix*, since they carry the same set of conserved quantum numbers, once the electroweak symmetry has been broken. In fact, this is possible, as was first pointed out in Ref. [5] and has been discussed by many others [5–7]. Before proceeding further, it may be noted that there are several phenomenological models with fermions and gauge bosons accessing the bulk [8–12], which have better control over the flavour problem. In these models, the top quark remains close to the TeV brane along with the Higgs field while the other fermions are close to the UV brane. This suppresses the higher-dimensional operators contributing to flavour-changing neutral currents, since the effective interaction of fermions with the Higgs field is governed by the overlap of their profiles and hence this scenario naturally generates the pattern of fermion masses and mixings. These models predict heavy Kaluza-Klein particles on the TeV brane having masses in the range of a TeV. However, the radion and Higgs fields, being still close to the TeV brane, mix more-or-less without bulk effects [13]. Hence, the mixing can be understood fairly accurately using a minimal model where all the relevant particles are confined to the TeV brane⁶, for this is, after all, no more than approximating a sharply-peaked function by a delta function.

In the following section, therefore, we briefly discuss, following Refs. [6, 7] how the radion-Higgs field mixing may be described in terms of a single mixing parameter ξ . The next section then describes constraints on the mixed Higgs-Radion scenario, as obtained using all experimental inputs currently available, especially those from the LHC. For easy comparison, we include projections of the discovery reach of the LHC alongside the current constraints. Before concluding, we include a short section on the so-called ‘conformal point’ near $\xi = 1/6$, which has unique features. While some of the observations in this paper echo previous ones [14], the data used are current, leading to new bounds, and, for ease of reading, we have presented our findings in a manner such that this paper can be read as far as possible independently of the preceding literature.

2. RADION-HIGGS MIXING

Mixing of the radion field $\varphi(x)$ with the Higgs scalar $h(x)$ of the SM has been discussed by several authors [5–7], with the same broad features, but we choose to closely follow the formalism of Ref. [6, 7].

⁶The only caveat to this is the fact that heavy Kaluza-Klein excitations of the top quark may contribute to Higgs production at a hadron collider through loop diagrams. However, if these excitations are at the level of a TeV, the corresponding loop contributions are not more than a few percent and may be safely neglected — as we have done in this work.

The mixing occurs through the kinetic terms

$$\mathcal{L} = \frac{1}{2}\partial^\mu h \partial_\mu h - \frac{1}{2}M_h^2 h^2 + \frac{\beta}{2}\partial^\mu \varphi \partial_\mu \varphi - \frac{1}{2}M_\varphi^2 \varphi^2 + 6\gamma\xi \partial^\mu \varphi \partial_\mu h \quad (12)$$

where $\gamma \equiv v/\Lambda_\varphi$, v being the SM Higgs vacuum expectation value. In this formalism, the mixing parameter appears twice – once in the mixing term $6\gamma\xi \partial^\mu \varphi \partial_\mu h$, and once in the non-canonical normalisation $\beta \equiv 1 + 6\gamma^2\xi$ of the radion kinetic term. As is usual, the Higgs boson mass is given by $M_h^2 = 2\lambda v^2$, where λ is the Higgs quartic coupling and v is the Higgs vacuum expectation value.

We note that the presence of the non-canonical normalisation β means that the identification of physical states H and Φ will involve a scaling as well as a rotation of states, i.e. a non-unitary transformation. Hence, we write the unphysical states φ, h as linear combinations of the physical ones Φ, H , with real coefficients A, B, C and D , thus

$$\begin{aligned} \varphi &= A\Phi + BH \\ h &= C\Phi + DH, \end{aligned} \quad (13)$$

where the coefficients A, B, C and D are given by

$$\begin{aligned} A &= -\frac{1}{Z}\cos\theta & B &= \frac{1}{Z}\sin\theta \\ C &= \sin\theta + \frac{6\gamma\xi}{Z}\cos\theta & D &= \cos\theta - \frac{6\gamma\xi}{Z}\sin\theta \end{aligned} \quad (14)$$

in terms of

$$Z^2 = \beta - (6\gamma\xi)^2 \quad (15)$$

and a mixing angle θ , defined by

$$\tan 2\theta = \frac{12\gamma\xi Z M_h^2}{M_\varphi^2 - M_h^2 (Z^2 - 36\gamma^2\xi^2)} \quad (16)$$

The mixing parameter ξ is immediately constrained by the requirement that $Z^2 > 0$ to get a real mixing angle. The mass eigenvalues of the physical eigenstates Φ and H are now given by

$$M_{\Phi, H}^2 = \frac{1}{2Z^2} \left(M_\varphi^2 + \beta M_h^2 \pm \sqrt{(M_\varphi^2 + \beta M_h^2)^2 - 4Z^2 M_\varphi^2 M_h^2} \right) \quad (17)$$

where the sign is chosen to ensure that $M_H < M_\Phi$. We identify the lighter state H as the scalar state of mass around 125 GeV which was discovered at the CERN LHC in 2012, while

the other state Φ is a heavier scalar state predicted in the model. From these formulae, it is clear that the free parameters in question are M_h , M_φ , Λ_φ and ξ , everything else being computable in terms of them. We also note in passing that since $M_h^2 = 2\lambda v^2$, this makes the Higgs quartic coupling λ an unknown quantity in this model, just as it used to be in the Standard Model before the identification of the 125 GeV scalar with the Higgs boson⁷.

Instead of the Lagrangian parameters M_h and M_φ , however, we find it more convenient to use the physical masses M_H and M_Φ , which can be traded for the previous two by some simple algebra, leading to

$$\begin{aligned} M_\varphi^2 &= \frac{Z^2}{2} \left[M_\Phi^2 + M_H^2 + \sqrt{(M_\Phi^2 + M_H^2)^2 - \frac{4\beta M_\Phi^2 M_H^2}{Z^2}} \right] \\ M_h^2 &= \frac{Z^2}{2\beta} \left[M_\Phi^2 + M_H^2 - \sqrt{(M_\Phi^2 + M_H^2)^2 - \frac{4\beta M_\Phi^2 M_H^2}{Z^2}} \right] \end{aligned} \quad (18)$$

Since we identify $M_H = 125$ GeV, we are left with a set of only three independent parameters, viz. M_Φ , Λ_φ and ξ . The rest of our analysis will be presented in terms of these variables.

We now have another theoretical constraint, apart from $Z^2 > 0$. This is the requirement that the parameters M_φ and M_h be real (to keep the Lagrangian Hermitian), which automatically means that

$$(M_\Phi^2 + M_H^2)^2 > \frac{4\beta M_\Phi^2 M_H^2}{Z^2} \quad (19)$$

Imposing both these constraints reduces the possible range of ξ , for a given M_Φ and Λ_φ , quite significantly (see below).

Since the mixing of the h and the φ to produce the physical H and the Φ is non-unitary, we define two mixing indicators as follows. We first invert Eq. (20) to write

$$\begin{aligned} \Phi &= a\varphi + bh \\ H &= c\varphi + dh, \end{aligned} \quad (20)$$

where

$$\begin{pmatrix} a & b \\ c & d \end{pmatrix} = \begin{pmatrix} A & B \\ C & D \end{pmatrix}^{-1}. \quad (21)$$

⁷This is a reflection of the fact that we still do not have a direct measurement of λ . All that we have is the estimate $\lambda = (125 \text{ GeV})^2/2v^2 \simeq 0.129$ — which is true only if the 125 GeV state is purely a SM Higgs boson without any admixture of new states.

In terms of this, we now define indicators

$$f_{\varphi/H} = \frac{|c|}{|c| + |d|} \quad f_{h/\Phi} = \frac{|b|}{|a| + |b|} \quad (22)$$

which, in a sense, indicate the fraction of radion φ in the light state H , and the fraction of Higgs boson h in the heavy state Φ . These, together with the mixing angle θ defined in Eq. (16), are plotted in Fig. 1, as a function of the mixing parameter ξ .

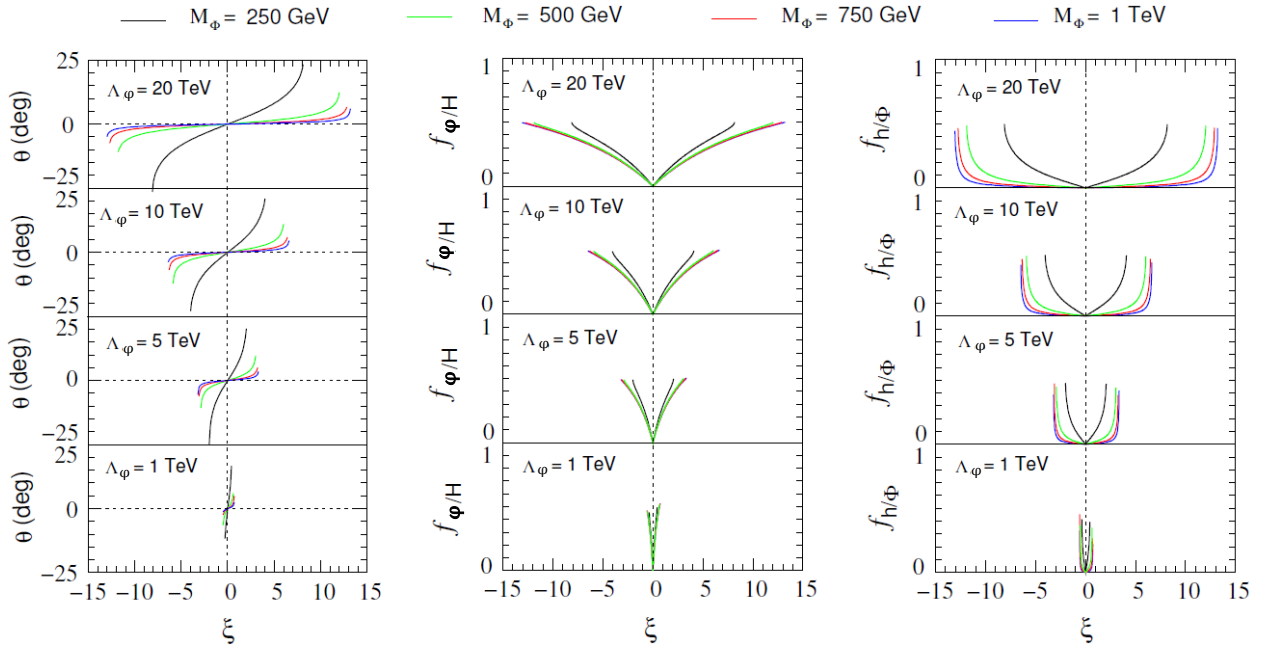


Figure 1: The variation with ξ of the mixing parameters (a) θ , (b) $f_{\varphi/H}$ and (c) $f_{h/\Phi}$. In each panel, the four boxes, from bottom to top, show the behaviour when $\Lambda_\varphi = 1, 5, 10$ and 20 TeV respectively, as marked. Inside the boxes, the curves are coloured black, green, red and blue for $M_\Phi = 250$ GeV, 500 GeV, 750 GeV and 1 TeV respectively. Observe that all these parameters vanish when $\xi = 0$, as expected. The lines break off abruptly for larger values of $|\xi|$ because of the theoretical constraints discussed in the text.

In each of the three panels in Fig. 1, we have four boxes placed one above the other, corresponding to choices of four different values of the radion vacuum expectation value, viz. $\Lambda_\varphi = 1, 5, 10$ and 20 TeV respectively (marked in the respective boxes). Within each box, the curves are colour-coded, with black, green, red and blue indicating benchmark choices of the heavy scalar mass as $M_\Phi = 250$ GeV, 500 GeV, 750 GeV and 1 TeV respectively (indicated at the top of the figure). Each curve ends abruptly at some maximum and minimum values of the mixing parameter ξ – this is a reflection of the theoretical limitations (see above). As may be seen from the different plots, this restriction is extremely stringent when Λ_φ is small, and even when we push Λ_φ as high as 20 , does not permit the value of $|\xi|$ to exceed 15 . If we consider the panel on the left, it is clear that we get significant values of the mixing angle

θ only when the heavy Φ state is as light as around 250 GeV. For values of M_Φ of 500 GeV or greater, θ does not exceed 10^0 . However, since the mixing is not unitary, the smallness of θ is not necessarily an indicator of small mixing. This becomes clear if we look at the central and right panels of Fig. 1, which tell us the proportion of the radion in the 125 GeV state, and the proportion of the Higgs boson in the heavier state respectively. In each case, as $|\xi|$ increases, the mixing becomes more, starting from zero when $|\xi| = 0$ to about equal mixtures when $|\xi|$ reaches its maximum theoretically-permitted value. The purpose of this paper is, as explained above, to see how far such large mixings are allowed in the light of current experimental data.

We next consider the effect of mixing on the couplings of the two scalar states to the SM fields. As shown in Ref. [7], the tree-level couplings of the heavy Φ state to pairs of SM fields $X\bar{X}$ (except $X = H$) have the form

$$g_{\Phi X\bar{X}} = g_{\varphi X\bar{X}} (C + \gamma A) \equiv c_\Phi g_{\varphi X\bar{X}} \quad (23)$$

where $g_{\varphi X\bar{X}}$ can be read off from Eqs. (9–10), and $c_\Phi = C + \gamma A$ is a scaling factor. Similarly, the couplings of the light 125 GeV state have the form

$$g_{HX\bar{X}} = g_{hX\bar{X}} (D + \gamma B) \equiv c_H g_{hX\bar{X}} \quad (24)$$

where $g_{hX\bar{X}}$ are the SM couplings and $c_H = D + \gamma B$ is a scaling factor. Very different from these is the coupling of the heavy scalar to a pair of light scalars, since all three fields are mixed states, and this can be written [7] for a $\Phi(p) - H(k_1) - H(k_2)$ vertex, as

$$g_{HH} = \frac{1}{\Lambda_\varphi} [(k_1^2 + k_2^2) \{AD^2 + 6\xi B(CD + \gamma AD + \gamma BC)\} + D \{12\gamma\xi AB + 2BC + (6\xi - 1)AD\} p^2 - 4M_h^2 D(AD + 2BC) - 3M_h^2 CD^2/\gamma] \quad (25)$$

The couplings of the scalars H and Φ with other particles are conveniently listed in the Appendix of Ref. [7].

To get a feeling of how these couplings are affected by the variation in the basic parameters ξ , Λ_φ and M_Φ , we plot them in Fig. 2 on a scheme similar to that in Fig. 1. The three panels show, from left to right, the scaling factors c_Φ and c_H , and the coupling g_{HH} respectively. As in Fig. 1 it is immediately clear that for $\xi = 0$, c_Φ is very small (small enough to appear as zero on this scale), as befits a radion with a small coupling to matter, whereas $c_H = 1$ indicating that the lighter scalar is the SM Higgs boson. Similarly, for $\xi = 0$, the g_{HH}

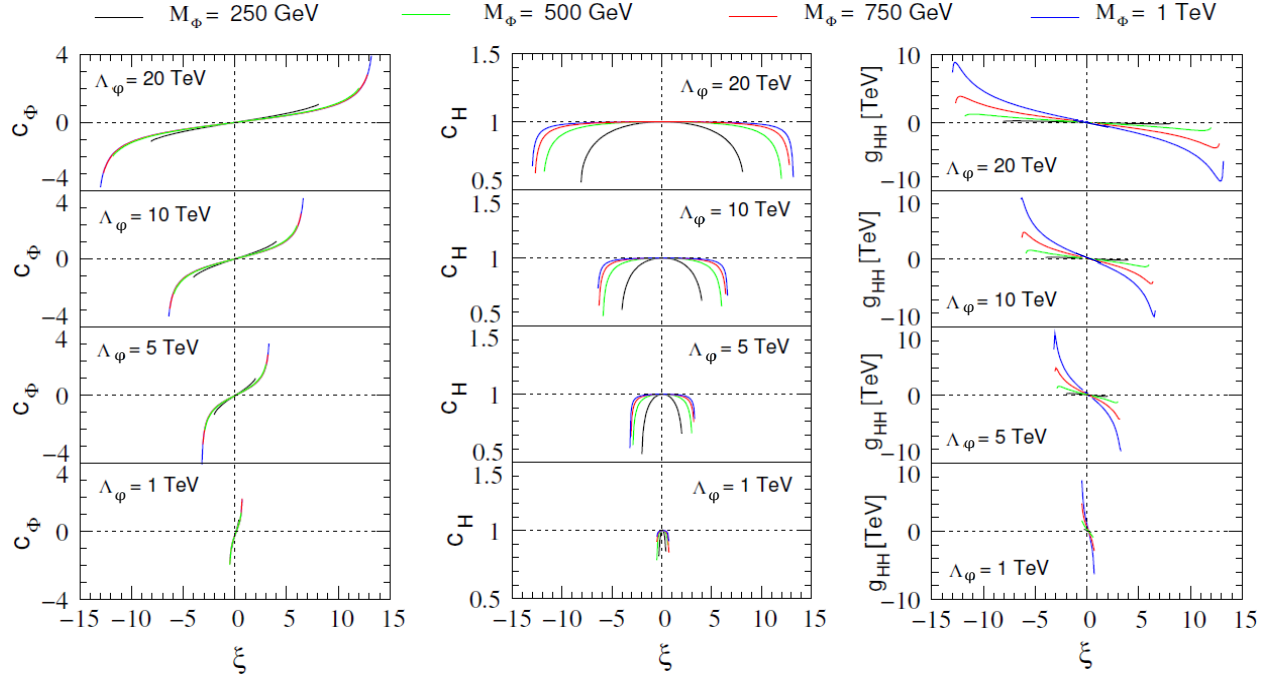


Figure 2: The variation with ξ of the (dimensionless) scaling factors (a) c_Φ and (b) c_H is shown in the left and central panels, while the right panel shows the ΦHH coupling g_{HH} , in units of TeV. The layout and colour conventions of this figure closely follow those of Fig. 1.

coupling is very small (small enough to appear as zero on this scale), indicating that the heavy scalar couples only weakly to a pair of light scalars. There are also genuine zeroes in the couplings, which are discussed in more detail in Section 4.

An interesting feature of both Fig. 1 and Fig. 2 is the fact that the variation in parameters is rather slow for smaller values of ξ , but is very sharp for larger values just before the unphysical region. These larger values of the scaling factor and ΦHH coupling are likely to have phenomenological consequences at observable levels, and hence are more likely to be constrained by experimental data. In the next section, we shall see that this is indeed the case.

3. EXPERIMENTAL CONSTRAINTS

We are now in a position to apply the experimental constraints to this model. Since the two scalars H and Φ are the crucial elements, the main constraints will come from

- (a) the measured signal strengths μ_{XX} of the 125 GeV scalar in its decay channels to $X\bar{X}$ pairs – these are known to match reasonably closely to the SM predictions, leaving only limited room for a mixed state;

- (b) the lack of signals for a heavy scalar in the range of a few hundred GeV to about a TeV – by implication, any new scalar would be very heavy and mix only marginally with the SM Higgs boson.

In principle, the scalars could also contribute as virtual states to any neutral current processes. However, as most of these are suppressed by the small masses of the initial states (either e^\pm or u and d quarks), we do not really get any useful constraints from these processes. Constraints from electroweak precision tests are not very strong [6, 15]. In the rest of this sections, therefore, we concentrate on the two issues listed above.

Signal Strength	8 TeV limits	13 TeV limits
$\mu_{\gamma\gamma}$	0.68 – 1.70 [16]	$\begin{cases} 0.31 – 1.27 [17] \text{ (CMS)} \\ 0.03 – 1.17 [18] \text{ (ATLAS)} \end{cases}$
μ_{WW}	0.58 – 1.42 [16]	—
μ_{ZZ}	0.76 – 2.16 [16]	0.78 – 1.62 [19] (CMS)
$\mu_{\tau\tau}$	0 – 2.26 [16]	—
μ_{bb}	0 – 3.13 [16]	0 — 1.23 (ATLAS)

Table 1: LHC results on the Higgs signals strengths at 95% confidence level. The 8 TeV limits are from ATLAS and CMS combined. Production is through gluon fusion, except for the last entry, which is through vector boson fusion.

We first take up the signal strengths of the 125 GeV scalar H . This decays into several channels

$$H \longrightarrow X + \bar{X} \tag{26}$$

where $X = \ell^-, u, d, s, c, b, W, Z, \gamma, g$ with one of X or \bar{X} being off-shell in the case of W and Z . At the LHC, the H is produced dominantly through gluon-gluon fusion⁸. Hence, we can define signal strengths μ_{XX} as

$$\mu_{XX} = \frac{\sigma(pp \rightarrow gg \rightarrow H)_{\text{exp}} \mathcal{B}(H \rightarrow X\bar{X})_{\text{exp}}}{\sigma(pp \rightarrow gg \rightarrow H)_{\text{SM}} \mathcal{B}(H \rightarrow X\bar{X})_{\text{SM}}} \tag{27}$$

where σ and \mathcal{B} stand for cross-section and branching ratio respectively, and the subscripts ‘SM’ and ‘exp’ mean the SM prediction and the experimental value respectively. If we are making a theoretical prediction, then ‘exp’ will stand for the expected value in the theoretical model in question — in the present case, the model with radion-Higgs mixing. Of course, in an experiment only the entire numerator on the right side of Eq. (27) can be measured and not the individual factors. By this definition, then, all the SM signal strengths are normalised

⁸In our numerical analysis, we have also included the vector boson fusion mode.

to unity, and experimental deviations from it constitute the leeway for new physics. These allowed experimental deviations are given in Table 1.

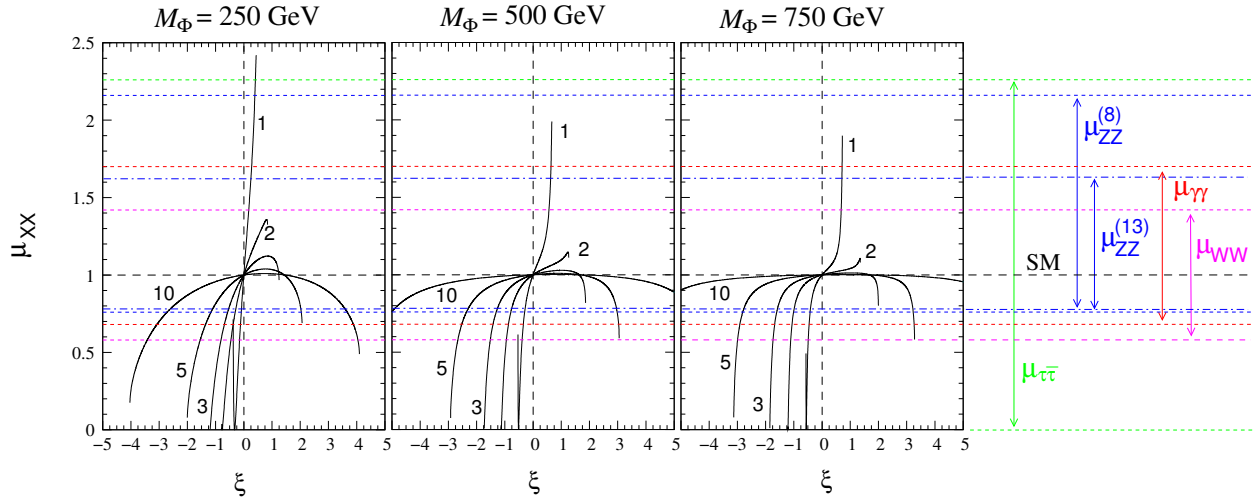


Figure 3: The variation of the predicted signal strengths with the mixing parameter ξ , for different choices of Λ_φ (in TeV), marked alongside each curve. Each panel corresponds to a different mass M_Φ as marked. The experimental constraints at 95% C.L. are shown on the right. Superscripts (8) and (13) indicate results from Run-1 and Run-2 respectively of the LHC.

Obviously, for zero mixing, the signal strengths predicted for the H scalar will be the same as the SM values, i.e. unity. As ξ increases, we should expect deviations from unity, and indeed that is what happens, as illustrated, in Fig. 3. The three panels, from left to right, correspond to choices of $M_\Phi = 250, 500$ and 750 GeV respectively. The graph for $M_\Phi = 1$ TeV is very similar to that for $M_\Phi = 750$ GeV, and hence we do not show it explicitly. Likewise, the actual graphs for $\mu_{\gamma\gamma}$ are slightly different, but not enough to show up on a plot at this scale. Each curve in the panels corresponds to the value of Λ_φ , in TeV, written alongside, i.e. 1, 2, 3, 5 and 10 TeV respectively. The steepness of the curves decreases with increasing Λ_φ , for which we also have larger permitted ranges in ξ , as we have earlier shown in Fig. 2. Horizontal broken lines in Fig. 3 represent the useful 95% C.L. constraints from the signal strengths in Table. 1, and are marked on the right side of the figure.

The behaviour of the predicted signal strengths with increasing ξ is quite as expected, remaining close to the SM value for small ξ and showing large deviations near the edge of the theoretically-allowed range. This, as we have seen earlier, is due to the large deviations of the coupling of the H from the SM coupling at such values of ξ . It is thus obvious that the present constraints from signal strengths will only affect narrow strips of the parameter space adjacent to the theoretically-disallowed region, and this, in fact, is what we find (see below). It may be noted in passing that a region of the parameter space where $D + \gamma B \simeq 0$ would be very strongly constrained from the signal strengths, but this does not happen anywhere

inside the region allowed by theoretical considerations.

When we turn to the heavy Φ state, once again the main production mode is through gluon-gluon fusion, but now there is no analogous SM prediction and hence one looks for the direct signals in the various decay channels of the Φ . As in the case of the light scalar, the potentially observable ones are $\Phi \rightarrow \gamma\gamma$ [20–22], WW [23–26], ZZ [24,27–29] and $\tau^+\tau^-$ [30–33] to which we can now add $\Phi \rightarrow t\bar{t}$ and $\Phi \rightarrow HH$ [34–37]. The $b\bar{b}$ [38] signal would be difficult to distinguish from the QCD background, unless the mass of the Φ scalar is very well known, as in the case of the H scalar. The behaviour of all these branching ratios, as functions of the scalar mass M_Φ is shown in Fig. 4, where Λ_φ is fixed to 5 TeV and the panels, from left to right, correspond to $\xi = 0$ (no mixing), and $\xi = 1, 2$ and 3 respectively. The relevant decay channel is marked alongside each curve. These curves terminate at the left end where they correspond to theoretically-disallowed regions in the parameter space.

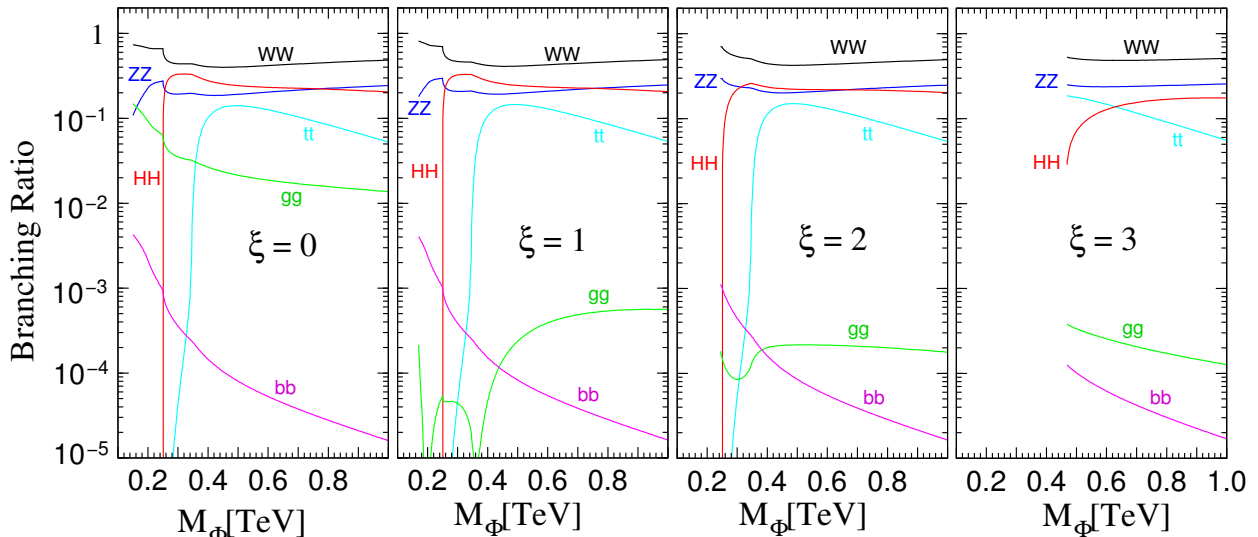


Figure 4: Two-body branching ratios of the heavy scalar Φ as a function of its mass M_Φ , for different choices of the mixing parameter $\xi = 0, 1, 2$ and 3. The extreme left panel, viz. $\xi = 0$, corresponds to a pure radion state. Branching ratios for the diphoton channel are not shown as they are too small to appear on the chosen scale. For these plots, we have set $\Lambda_\varphi = 5$ TeV. Variation with Λ_φ exists, but is slight.

One feature which is immediately obvious from these curves is the fact that the scalar Φ decays dominantly through the WW and ZZ channels. When the mixing is low, the HH channel is also competitive, but as ξ rises, it gets suppressed. In any case, the signals from the WW and ZZ channels are leptonic and clean, whereas the signals arising from HH , dominantly leading to $4b$ final states, are hadronic, as are those arising from the direct decays of the Φ into quark pairs. These hadronic channels are generally suppressed compared to WW and ZZ , and, in any case, would be plagued by large QCD backgrounds. It may

be still possible to investigate the $t\bar{t}$ and HH channels, using jet substructure-based tagging methods for boosted particles, but such experimental searches are still not competitive [39]. Thus, in principle, we get constraints from every decay channel of the Φ , but the most useful ones will arise from the ATLAS and CMS search results for a heavy scalar resonance decaying to WW and ZZ pairs, which are equally applicable to the Φ scalar in the model under consideration. As is well-known, the experimental results are all negative, and hence the 95% C.L. upper limits on the cross-section are given in Table 2.

$pp \rightarrow S \rightarrow WW$	$M_S = 250$ GeV	$M_S = 500$ GeV	$M_S = 750$ GeV	$M_S = 1$ TeV
ATLAS (Run I) [23]	—	0.191	0.039	0.020
CMS (Run I) [24]	1.590	0.287	0.221	0.064
ATLAS (Run II) [25]	—	0.884	0.253	0.066
CMS (Run II) [26]	51.395	4.866	2.882	1.708
$pp \rightarrow S \rightarrow ZZ$	$M_S = 250$ GeV	$M_S = 500$ GeV	$M_S = 750$ GeV	$M_S = 1$ TeV
ATLAS (Run I) [27]	0.298	0.044	0.012	0.011
CMS (Run I) [24]	0.110	0.089	0.040	0.025
ATLAS (Run II) [28]	0.758	0.111	0.068	0.050
CMS (Run II) [29]	0.416	0.136	0.070	0.060

Table 2: LHC 95% upper limits on the cross-section, in pb, for a heavy scalar S decaying to a WW or a ZZ pair, for the benchmark values $M_S = 250, 500, 750$ and 1000 GeV respectively. In our work, we have used only the Run-2 data for the constraints.

We are now in a position to compare these data with the predictions of our theory. As in the case of the H state, the cross section for $pp \rightarrow \Phi \rightarrow VV$, where $V = W, Z$, can be written

$$\sigma(pp \rightarrow \Phi \rightarrow VV) = \sigma(pp \rightarrow gg \rightarrow \Phi) \mathcal{B}(\Phi \rightarrow VV) \quad (28)$$

where $\mathcal{B}(\Phi \rightarrow VV)$ is the branching ratio of the Φ to a VV pair. These can be calculated in terms of the free parameters ξ , M_Φ and Λ_φ respectively. Our results are shown in Fig. 5.

The four upper panels of Fig. 5 represent the cross-section, in pb, for the process $pp \rightarrow \Phi \rightarrow WW$ and the lower four panels represent the process $pp \rightarrow \Phi \rightarrow ZZ$. In each row the panels correspond, from left to right, to $M_\Phi = 250$ GeV, 500 GeV, 750 GeV and 1 TeV,

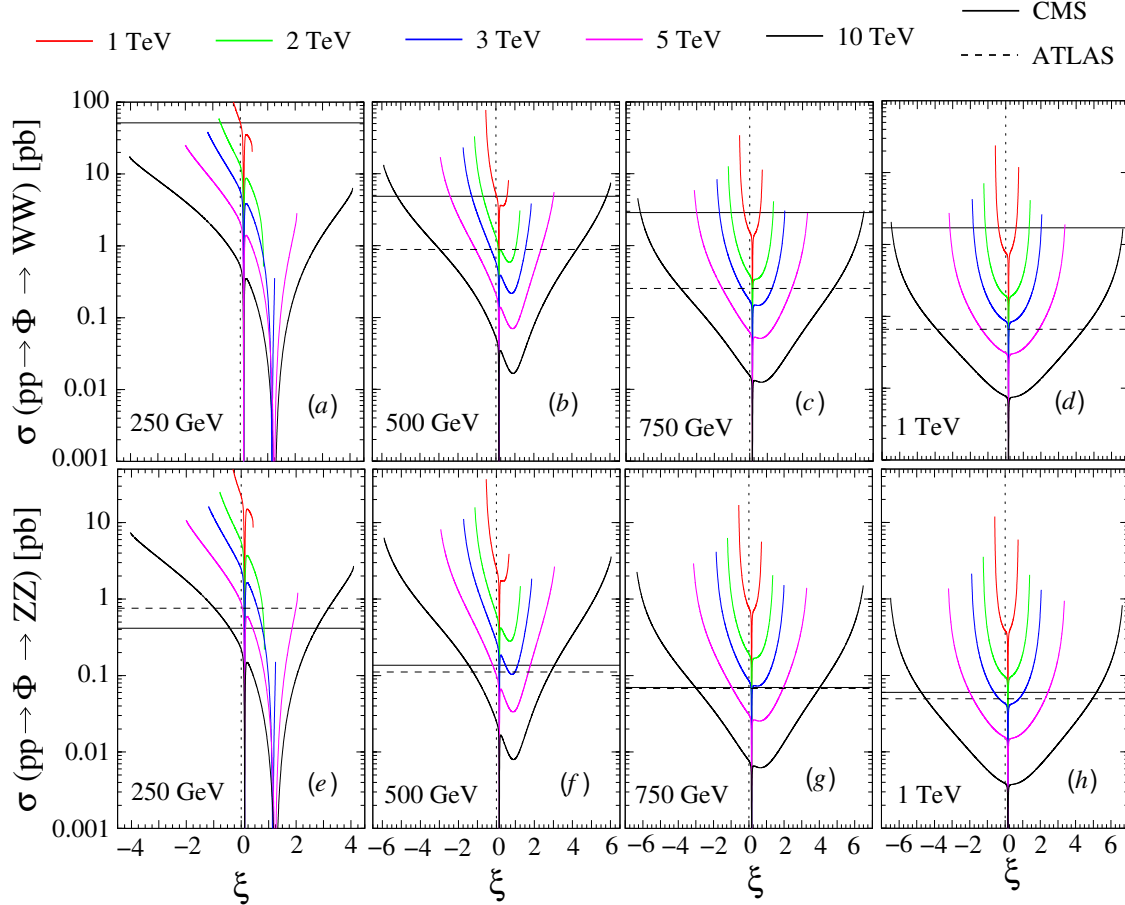


Figure 5: Predictions of this model vis-à-vis LHC searches for a heavy ‘SM-like’ scalar. The upper set of panels are for a WW final state and the lower set of panels are for a ZZ final state. Each panel shows the variation with ξ for a definite M_Φ as marked, and the different curves correspond to different values of Λ_φ , as indicated in the legend above the panels. Horizontal solid (dashed) lines indicate the 95% C.L. CMS (ATLAS) 13 TeV constraints as in Table 2.

respectively. Within each panel, the curves show the variation of the cross-section with the mixing parameter ξ , for different values of the radion vacuum expectation value, corresponding to different colours, as marked in the legend above the panels. The horizontal solid lines correspond to the CMS bounds from the 13 TeV data, as shown in Table. 2, while the broken lines correspond to the ATLAS 13 TeV data.

All the curves have a distinct minimum at a small value of ξ varying from 0.2 to 2 — this corresponds to a minimum in the cross-section $\sigma(pp \rightarrow gg \rightarrow \Phi)$ where there is maximal cancellation in the amplitude for $gg \rightarrow \Phi$ due to the top quark loop and the trace anomaly term. In this region, the heavy scalar can be produced in association with a W^\pm/Z and it further decays to WW or ZZ pairs, leading to a final state with three gauge bosons or their decay products. In view of the low production cross-sections for higher values of Λ_φ , one has to consider hadronic decays of one or more of these gauge bosons, and this immediately

invites a large QCD background at the LHC. However, the region can be successfully probed at a high energy e^+e^- collider (such as the proposed ILC) with $\sqrt{s} = 1$ TeV [40].

In addition to the dip described above, there is a very sharp minimum, very close to the vertical axis, which corresponds to the so-called ‘conformal’ point, where $c_\Phi \rightarrow 0$. We defer the discussion of this point to the next section and focus here on the constraints obtainable from the rest of the parameter space. Here, as in the case of signal strengths the constraints rule out larger values of ξ , with the exact bound depending on the other two parameters of the theory.

From Figs. 3 and 5 we can draw some general conclusions. The first is that the effect of increasing the mixing parameter ξ becomes weaker and weaker as the vacuum expectation value Λ_φ keeps increasing. This is true both for the signal strengths in Fig. 3 as well the cross-section in Fig. 5 and is easy to track down as due to the limiting case $\gamma \rightarrow 0$. A similar argument may be made for the parameter M_Φ – at least numerically – though the parameter dependence here is much more complicated. We may argue, therefore, that for a fixed ξ , the region with small M_Φ and small Λ_φ is more constrained — which also corresponds to the commonsense argument that if these parameters are small, radion-mediated processes are large and vice versa. These expectations are corroborated by our results shown in Fig. 6. Here we show the Λ_φ – M_Φ plane for four different values of ξ , viz. $\xi = -0.5, 0, 1$ and 1.5 , as marked on each panel. As indicated in the key at the top, the region shaded grey corresponds to the theoretically disallowed region, and includes all values of $\Lambda_\varphi < 1$ TeV, except in the panel on the top left, marked $\xi = 0$, which corresponds to the case of an un-mixed radion of mass M_Φ . Here, though values of $\Lambda_\varphi < 1$ TeV are theoretically permitted, the experimental constraints do not allow them, as is apparent from the figure. In all the panels, the dark grey shaded region is ruled out by the signal strengths at Runs 1 and 2 and the hatched regions by the ATLAS and CMS searches for a heavy scalar at Run-2 of the LHC. These are the strongest constraints and represent the state of the art as far as current experimental data are concerned⁹. The jagged shape of the curves reflects the fact that the LHC has, till now, collected quite a small amount of data for rare processes like the decay of a heavy scalar. However, the LHC has the potential to search much further, and this is shown by the red and yellow-shaded regions, which represent, respectively, the expectations from the signal strength measurements if $\mu_{XX} = 1 \pm 0.05$ for all X , and the ATLAS and CMS discovery limits at 95% C.L. for the heavy Φ if the LHC were to run at 14 TeV and collect 3000 fb⁻¹ of data [41, 42] — which may not be too far from the reality. For the panel with $\xi = 0$,

⁹We have, in fact, considered constraints from all the channels separately, but the others are subsumed in the ones shown in the figure, and hence are not shown in order to have uncluttered figures.

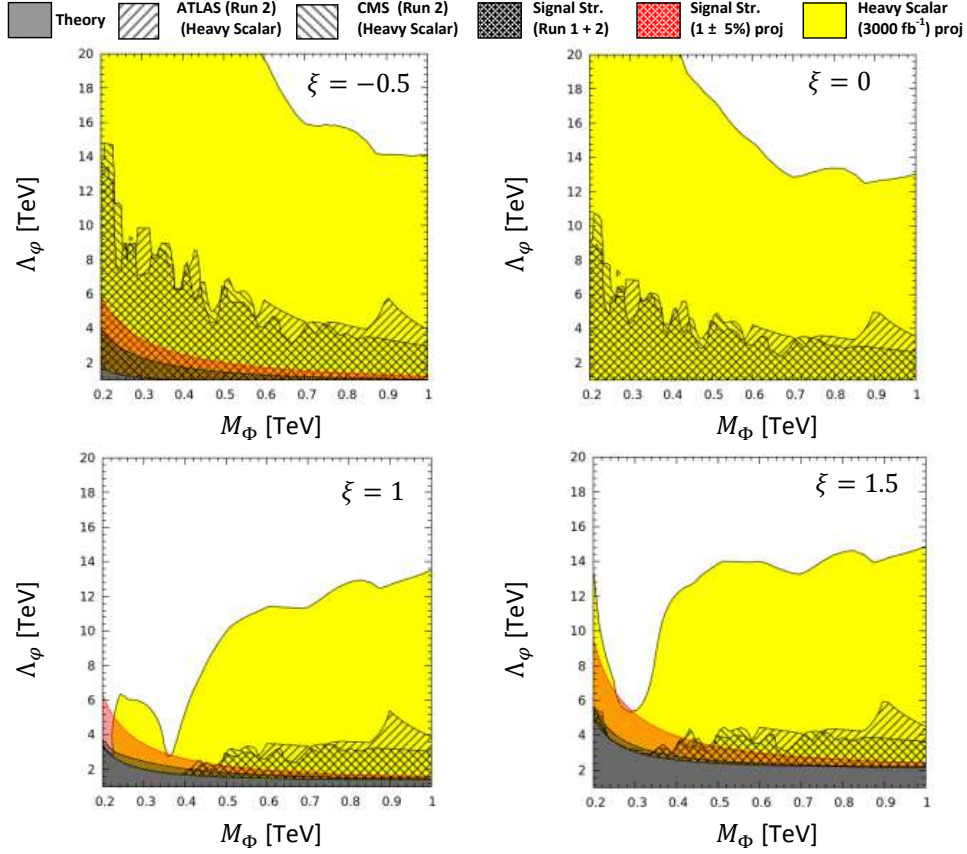


Figure 6: Constraints from LHC data on the Λ_ϕ - M_Φ plane for different values of the mixing parameter ξ . The region shaded grey is theoretically disallowed and the region shaded dark grey is ruled out by the Higgs boson signal strengths. Hatching with opposite slants correspond to the ATLAS and CMS constraints from the heavy scalar search. The red-shaded region represents a projection of constraints from the signal strengths, assuming $\mu_{XX} = 1 \pm 0.05$ for all channels. Finally, the yellow-shaded region represents a combination of the ATLAS and CMS projected discovery limits from the ZZ channel, assuming a data collection of 3000 fb^{-1} at 14 TeV.

there are no constraints from the signal strengths, since the H is completely SM-like; but the constraints from the heavy scalar searches are quite strong because that scalar is a pure radion. A comparative study of the four plots indicates that the value $\xi \approx 1$ would permit the largest part of the parameter space to survive consistently negative results from LHC, while negative values of ξ are better suited to a discovery of the heavy scalar predicted in this theory.

Coming to constraints on ξ , it is clear from Figs. 3 and 5 that $\xi = 0$, which corresponds to the 125 GeV scalar being the Standard Model Higgs boson — not surprisingly — is always allowed by the signal strength data. For given values of M_Φ and Λ_ϕ , ξ can range on the positive and negative side, but when its magnitude grows larger, all new physics effects

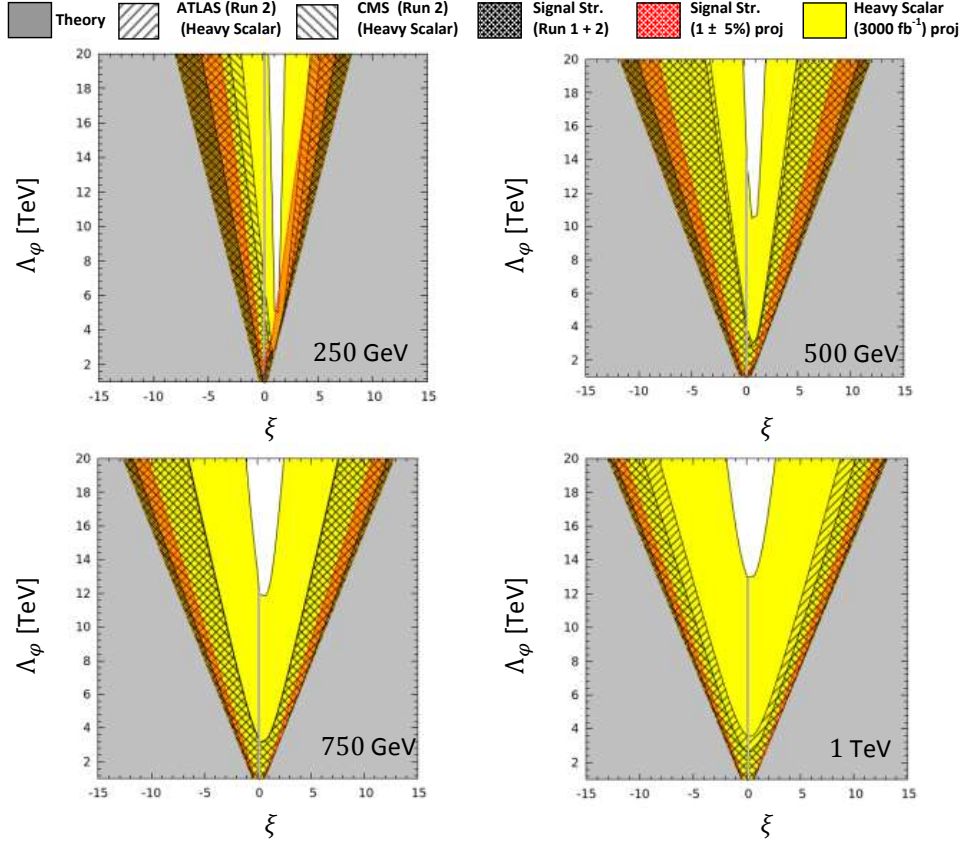


Figure 7: Constraints from LHC data on the Λ_φ - ξ plane for different values of the heavy scalar mass M_Φ . The region shaded grey is theoretically disallowed and the region shaded dark grey is ruled out by the Higgs boson signal strengths. Hatching with opposite slants correspond to the ATLAS and CMS constraints from the heavy scalar search. As in Fig. 6, the red-shaded region represents a projection of constraints from the signal strengths, assuming $\mu_{XX} = 1 \pm 0.05$ for all channels and the yellow-shaded region represents a combination of the ATLAS and CMS projected discovery limits, assuming a data collection of 3000 fb^{-1} at 14 TeV.

grow and, at some point, higher magnitudes of ξ get disallowed – first by the experimental constraints and then by the requirement of theoretical consistency. For low values of Λ_φ and M_Φ , we arrive at this point for fairly low values of ξ . As both these parameters increase, however, the allowed range grows, creating a funnel-like shape, which grows wider as Λ_φ and M_Φ increase. This is illustrated in Fig. 7, where we show the Λ_φ - ξ plane for the same choices of M_Φ as in the earlier figures. The shading and hatching conventions of this figure are exactly the same as those of Fig. 6. It is immediately obvious that for low values of Λ_φ close to 1 TeV, the range of ξ is severely constrained by theoretical consistency alone. A heavy scalar of mass 250 GeV is also rather severely constrained, except for a narrow cone, which will shrink further when the LHC finishes its run. Constraints ease up for a heavier scalar, since that is much more difficult to find. It is interesting that even if LHC completes its run without finding any evidence for a heavy scalar up to 1 TeV, there will be a range

of parameter space where this model is still allowed. However, for these parameters, the 125 GeV will be so similar to the SM Higgs boson, and the interactions of the heavy scalar will be so heavily suppressed that the model may no longer be interesting, at least from a phenomenological point of view.

An interesting feature of all the plots in Fig. 7 is the needle-thin sliver of allowed parameter space which appears in every graph close to the vertical axis. This corresponds, in every case, to the ‘conformal point’ mentioned above, where all constraints from a heavy scalar search weaken considerably. This region – though extremely fine-tuned – is interesting in its own right, and therefore we carry out a detailed study in the next section.

4. THE CONFORMAL POINT

As explained before, for every choice of M_Φ and Λ_φ , there is a fixed value $\xi = \xi_0$ which satisfies the equation $c_\Phi = 0$, and hence

$$C(\xi) + \gamma A(\xi) = 0 \tag{29}$$

and this is known as the ‘conformal’ point¹⁰. It corresponds to the case when the tree-level couplings $g_{\Phi X\bar{X}}$ of both the fermions and gauge bosons – generically denoted X – with the heavy scalar Φ vanish. This is a curious situation and corresponds to the case when the mixing is fine-tuned to be such that the parts of the coupling arising from the SM h and the radion φ cancel each other. Like all fine-tuned situations, if this is the reality, it can hardly be a random effect, and must represent some deeper structure in the theory, which is not addressed in our present formulation. Nevertheless, it is interesting to explore the phenomenological implications of this scenario. In this section, therefore, we investigate the conformal point and see how it can be constrained using current and projected data, just as the other points can. It is important to note that though most of the tree-level couplings of the Φ to pairs of SM particles vanish at the conformal point (except for the coupling to HH pairs), there exist one-loop couplings to pairs of gauge bosons through the trace anomaly. This makes the pattern of branching ratios at the conformal point very different from that in other regions of parameter space. The most important feature of this is the fact that the decays $\Phi \rightarrow gg$ and $\Phi \rightarrow \gamma\gamma$ are considerably enhanced with respect to the others – in fact the former is the dominant decay mode. This behaviour is nicely exhibited in Fig. 8, where we exhibit the behaviour of the relevant branching ratios in the immediate vicinity of the

¹⁰From this stage we drop the quotes on ‘conformal’.

conformal point.

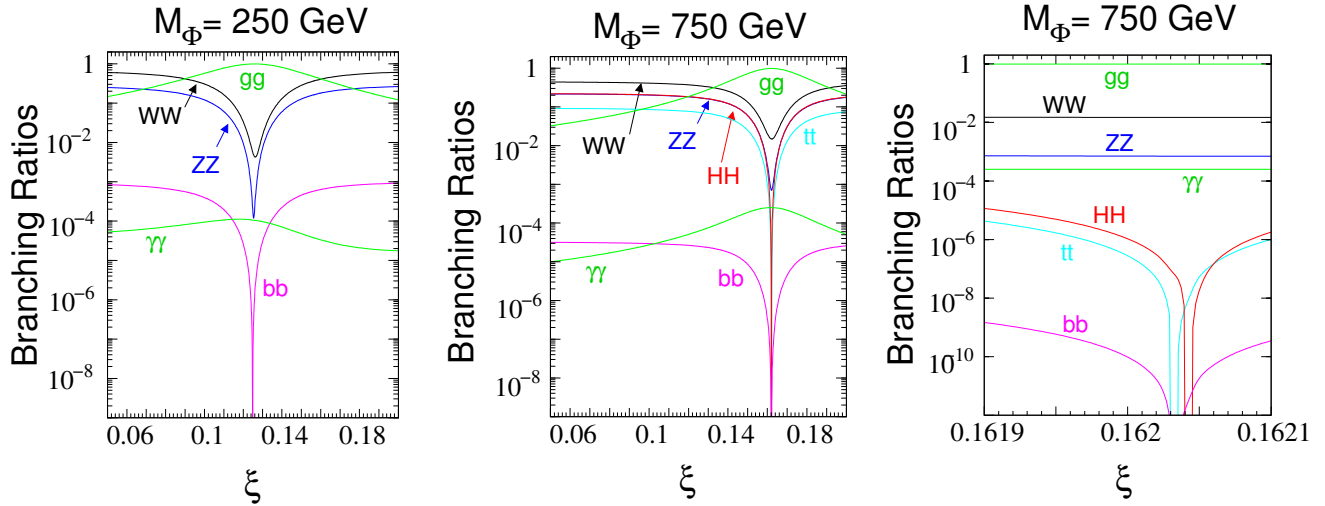


Figure 8: Branching ratios of the heavy scalar Φ in the neighbourhood of the conformal point. Note that the conformal point is quite sensitive to the value of M_Φ . There is some minor dependence on the radion vacuum expectation value Λ_φ , but for purposes of comparison it has been set at 2 TeV for every plot in this figure. The sharp drop in the tree-level decays at the conformal point may be noted. The conformal point for the decay $\Phi \rightarrow HH$ is close to, but different from that for other decays, as is clear in the panel on the right, which is a zoomed version of the central panel.

In Fig. 8, it is immediately apparent that for the particular value $\xi = \xi_0$, the tree-level decay modes of $\Phi \rightarrow X\bar{X}$, where X is a massive gauge boson or a fermion, drop sharply by many orders of magnitude. This is particularly true for the cases $X = t, b$ and H , with the minimum for the last case occurring at a slightly displaced point from the others (best seen in the zoomed panel on the right). On the other hand, the branching ratios for the purely one-loop decays, viz. $\Phi \rightarrow gg$ and $\Phi \rightarrow \gamma\gamma$ exhibit a growth at the same point, attributable to their partial decay widths being finite, whereas the others drop almost to zero. However, the decays to WW and ZZ states do not disappear altogether because they too have anomaly contributions. Naturally the decay $\Phi \rightarrow gg$ dominates the others because of the appearance of the strong coupling as well as the colour factor. The decay $\Phi \rightarrow \gamma\gamma$ also shows a gentle increase, but is intrinsically much more rare than the digluon mode. At the conformal point, therefore, constraints on the model will have to be sought in a different fashion. One obvious way is to consider Higgs boson signal strengths, for if the couplings of the Φ vanish that does not mean that the couplings of the H will also vanish. Accordingly, there will be contributions to the signal strengths and these can be used to constrain the model. In fact, even the heavy scalar searches, i.e. $pp \rightarrow S \rightarrow VV$, where $V = W, Z$ can be used to a limited extent, since the branching ratios $\Phi \rightarrow VV$, though small at $\xi = \xi_0$, are not absolutely negligible. However – and this is a distinct feature of the conformal point –

the strongest bounds come from diphoton searches, which is not entirely surprising, given that this mode is considerably enhanced at the conformal point.

In trying to understand how the conformal point is constrained by the data, we need to recognise that the conformal point ξ_0 is not unique, but a function of M_Φ and Λ_φ , with the dependence on the former being much stronger than that on the latter. Its variation with M_Φ is shown in the upper panel of Fig. 9, where the thickness of the line corresponds to variation of Λ_φ from 1 TeV to 20 TeV. This plot shows that the variation flattens out as M_Φ grows above 500 GeV, and has a very weak dependence on Λ_φ . Nevertheless, we have scanned a sizeable portion of the M_Φ - Λ_φ plane and calculated the values of ξ_0 at every point by solving Eq. (29).

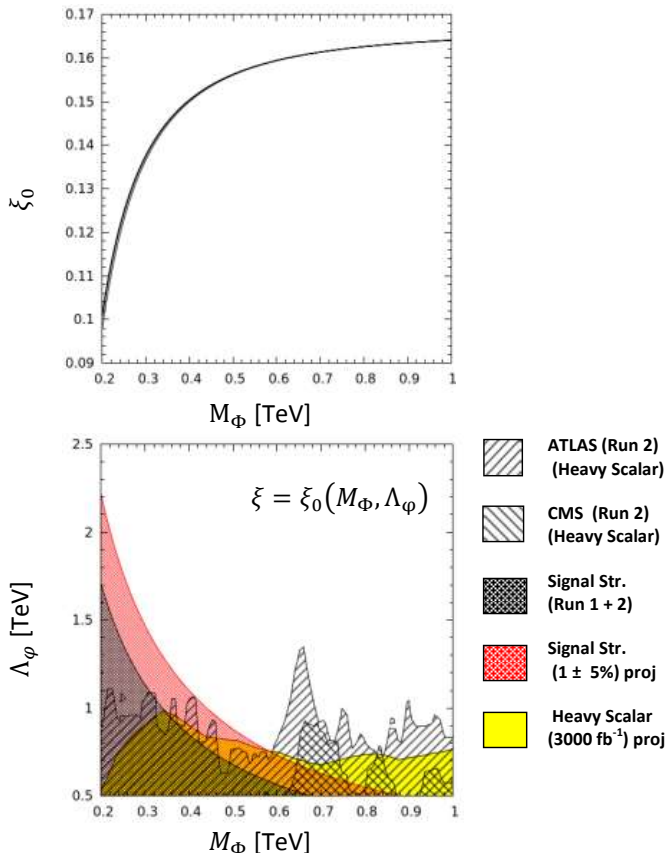


Figure 9: Constraints on the conformal point ξ_0 . The variation of ξ_0 with M_Φ is shown in the upper panel. The thickness of the line corresponds to variation of Λ_φ from 1 to 20 TeV. The lower panel shows the M_Φ - Λ_φ plane, assuming that at every point the mixing parameter $\xi = \xi_0$.

improvement can be obtained if these measurements yield results much closer to the SM prediction. The shaded yellow region represents the predictions from ZZ decay modes of a heavy scalar for the LHC running at 14 TeV with 3000 fb^{-1} [41, 42] of data (which is all

With these parameters, we now evaluate the measurables, viz. the signal strengths and the cross-sections for $pp \rightarrow S \rightarrow VV$, where $V = W, Z$. These are then compared with existing data to yield the constraints on the plane, as shown in the lower panel of Fig. 9. The conventions of this panel are exactly the same as those of Figs. 6 and 7, but the constraints follow a different pattern. As usual, low values of M_Φ and Λ_φ are excluded. However, there are no theoretical constraints, showing that there will always be a conformal point for any choice of model parameters. For small values of M_Φ , the strongest constraints come from the signal strengths (dark grey shaded area), while for higher values, it is the ATLAS and CMS data on diphotons – not WW and ZZ – from a heavy scalar resonance, which yield the best constraints. Projecting signal strength measurements at the level of $\mu_{XX} = 1 \pm 0.05$ for all X provides the red-shaded band, showing that moderate

that is currently available), and it does worse than the Run-2 data. It may be expected that diphoton searches would provide better discovery limits — when the Run-2 projections become available.

All in all, we can conclude that the conformal point is somewhat less constrained than the rest of the parameter space. It was this narrow window which had been used [43] to explain the purported discovery of a heavy 750 GeV scalar during 2015-2016 [44], though that proto-signal did not survive the test of time [21, 22].

5. SUMMARY AND OUTLOOK

The minimal Randall-Sundrum model continues to be one of the most elegant ways of solving the hierarchy problem, and it works best if there is a Goldberger-Wise stabilisation, which works best if there is a light radion state. Though there are strong constraints on such a light radion per se, there remains room for a light radion mixed with the SM Higgs boson to survive. In this article, we have explored this possibility, using an existing formalism, in the light of current data from the LHC Runs 1 and 2. Our findings are summarised below.

The possibility of a radion-Higgs mixing arises essentially because we have no independent measurement of the Higgs boson self coupling λ , so that the SM formula $M_h^2 = 2\lambda v^2$ is open to other interpretations. One of these is the mixed radion-Higgs scenario, where the lighter eigenstate is identified with the 125 GeV scalar discovered at the LHC. In this model, there are three free parameters, viz. the mixing parameter ξ , the mass M_Φ of the heavy scalar Φ , and the radion vacuum expectation value Λ_φ . However, self-consistency of the theory imposes fairly stringent constraints on the choices of the mixing parameter ξ . These, as we show, are further constrained by (a) the signal strengths measured for the decays of the 125 GeV scalar at the LHC, and (b) the search for a heavy scalar decaying into a pair of electroweak vector bosons, be they W 's, Z 's or photons. These lead to further bounds on the parameter space, essentially pushing Λ_φ above a TeV (and hence reducing all radion-mediated effects) and M_Φ to values closer to a TeV, though here some avenues for a lighter M_Φ remain.

In addition to the current data, we have tried to predict discovery limits at the LHC in two ways. One way is to use the signal strengths, and assume that they will eventually converge within 5% of the SM prediction. This leads to modestly enhanced bounds on the radion-Higgs mixing scenario. The other way is to use the projected discovery limits from the ATLAS and CMS Collaborations for a heavy scalar in Run-2, where we identify that heavy

scalar with our heavier eigenstate Φ . This, in fact, is very effective for most choices of the mixing parameter ξ and is sensitive to rather high values of M_Φ and Λ_φ . The only exception is at the so-called conformal point, which is a peculiar feature of this model, involving a value of the mixing parameter where the heavy scalar essentially decouples from SM fields. Even this is constrained, however, by the signal strengths and by the diphoton decay mode, which, being generated by the trace anomaly, survives the vanishing of tree-level couplings. However, the smallest values of M_Φ and Λ_φ are, indeed, allowed if this scenario were to be true.

It is interesting to ask how our results would be modified if we replace the simplistic model used above with a more phenomenologically-relevant model where the fields can access the bulk. As explained in the Introduction, the radion and Higgs fields, being still close to the TeV brane, mix in the same manner [13]. The decay of the radion to the light quarks is severely suppressed because of the small overlap [45] of their wavefunctions in the bulk. Decays of the radion to massive gauge bosons are governed by an additional coupling that can be safely neglected for $\Lambda_\varphi \gtrsim 1$ TeV. Radions decaying to massless gauge boson pairs (especially to diphotons) is significantly enhanced, however, due to the tree-level coupling in the case of bulk scenario. However, this doesn't really effect our region of interest [40]. We feel, therefore, that the results of this work are robust against more realistic variations of the minimal model and may be safely adopted in such cases.

To conclude, then, we have shown that a mixed radion-Higgs scenario is quite consistent with the current experimental data at the LHC, and there is every possibility that the heavy scalar predicted in this model could be discovered as the LHC continues to run at its present energy of 13 TeV. Discovery of this would certainly be one of the most exciting things to happen in the near future, and, if, the branching ratios turn out to be consistent with this model, could provide a powerful insight into the nature of spacetime itself. Such a happy consummation is to be devoutly hoped for, but, for the present, we must reconcile ourself to a fairly long wait as the Run-2 of the LHC continues.

Acknowledgements: The authors acknowledge useful discussions with Debjyoti Bardhan, Disha Bhatia and Abhishek Iyer. The work of SR was partly funded by the Board of Research in Nuclear Sciences, Government of India, under project no. 2013/37C/37/BRNS.

References

- [1] G. Aad *et al.* [ATLAS Collaboration], Phys. Lett. B **716**, 1 (2012); S. Chatrchyan *et al.* [CMS Collaboration], Phys. Lett. B **716**, 30 (2012).
- [2] L. Randall and R. Sundrum, Phys. Rev. Lett. **83**, 3370 (1999).
- [3] W. D. Goldberger and M. B. Wise, Phys. Rev. Lett. **83**, 4922 (1999).
- [4] See, for example, Z. Chacko, R. K. Mishra and D. Stolarski, JHEP **1309**, 121 (2013); B. Bellazzini *et al.*, Eur. Phys. J. C **73**, no. 2, 2333 (2013); Z. Chacko, R. K. Mishra, D. Stolarski and C. B. Verhaaren, Phys. Rev. D **92**, 056004 (2015); D. Elander and M. Piai, arXiv:1703.09205 [hep-th].
- [5] G. F. Giudice, R. Rattazzi and J. D. Wells, Nucl. Phys. B **595**, 250 (2001).
- [6] C. Csaki, M. L. Graesser and G. D. Kribs, Phys. Rev. D **63**, 065002 (2001).
- [7] D. Dominici *et al.*, Nucl. Phys. B **671**, 243 (2003).
- [8] S. J. Huber and Q. Shafi, Phys. Lett. B **498**, 256 (2001).
- [9] T. Gherghetta and A. Pomarol, Nucl. Phys. B **586**, 141 (2000).
- [10] Y. Grossman and M. Neubert, Phys. Lett. B **474**, 361 (2000).
- [11] K. Agashe, R. Contino, L. Da Rold and A. Pomarol, Phys. Lett. B **641**, 62 (2006).
- [12] A. M. Iyer, K. Sridhar and S. K. Vempati, Phys. Rev. D **93**, 075008 (2016).
- [13] C. Csaki, J. Hubisz and S. J. Lee, Phys. Rev. D **76**, 125015 (2007).
- [14] K. m. Cheung, Phys. Rev. D **63**, 056007 (2001); M. Chaichian, A. Datta, K. Huitu and Z. h. Yu, Phys. Lett. B **524**, 161 (2002); A. Datta and K. Huitu, Phys. Lett. B **578**, 376 (2004); P. K. Das, S. K. Rai and S. Raychaudhuri, Phys. Lett. B **618**, 221 (2005); H. de Sandes and R. Rosenfeld, Phys. Rev. D **85**, 053003 (2012); V. Barger, M. Ishida and W. Y. Keung, Phys. Rev. Lett. **108**, 101802 (2012); H. Kubota and M. Nojiri, Phys. Rev. D **87**, 076011 (2013); G. C. Cho, D. Nomura and Y. Ohno, Mod. Phys. Lett. A **28**, 1350148 (2013); N. Desai, U. Maitra and B. Mukhopadhyaya, JHEP **1310**, 093 (2013); P. Cox *et al.*, JHEP **1402**, 032 (2014); J. Cao *et al.*, JHEP **1401**, 150 (2014); D. W. Jung and P. Ko, Phys. Lett. B **732**, 364 (2014); H. Kubota and M. Nojiri, Phys. Rev. D **90**, no. 3, 035006 (2014); E. Boos *et al.*, Phys. Rev. D **90**, no. 9, 095026 (2014);

- S. Bhattacharya *et al.*, Phys. Rev. D **91**, 016008 (2015); P. R. Archer *et al.*, JHEP **1501**, 060 (2015); A. Efrati *et al.*, Phys. Rev. D **91**, no. 5, 055034 (2015); E. E. Boos *et al.*, Phys. Rev. D **92**, no. 9, 095010 (2015).
- [15] J. F. Gunion, M. Toharia and J. D. Wells, Phys. Lett. B **585**, 295 (2004).
- [16] G. Aad *et al.* [ATLAS and CMS Collaborations], JHEP **1608**, 045 (2016).
- [17] CMS Collaboration [CMS Collaboration], CMS-PAS-HIG-16-020.
- [18] The ATLAS collaboration [ATLAS Collaboration], ATLAS-CONF-2016-067.
- [19] CMS Collaboration [CMS Collaboration], CMS-PAS-HIG-16-041.
- [20] V. Khachatryan *et al.* [CMS Collaboration], Phys. Lett. B **750**, 494 (2015).
- [21] The ATLAS collaboration [ATLAS Collaboration], ATLAS-CONF-2016-059.
- [22] CMS Collaboration [CMS Collaboration], CMS-PAS-EXO-16-027.
- [23] G. Aad *et al.* [ATLAS Collaboration], JHEP **1601**, 032 (2016).
- [24] V. Khachatryan *et al.* [CMS Collaboration], JHEP **1510**, 144 (2015).
- [25] The ATLAS collaboration [ATLAS Collaboration], ATLAS-CONF-2016-062.
- [26] CMS Collaboration [CMS Collaboration], CMS-PAS-HIG-16-023.
- [27] G. Aad *et al.* [ATLAS Collaboration], Eur. Phys. J. C **76**, no. 1, 45 (2016).
- [28] The ATLAS collaboration [ATLAS Collaboration], ATLAS-CONF-2016-079.
- [29] CMS Collaboration [CMS Collaboration], CMS-PAS-HIG-16-033.
- [30] G. Aad *et al.* [ATLAS Collaboration], JHEP **1411**, 056 (2014).
- [31] CMS Collaboration [CMS Collaboration], CMS-PAS-HIG-14-029.
- [32] The ATLAS collaboration [ATLAS Collaboration], ATLAS-CONF-2016-085.
- [33] CMS Collaboration [CMS Collaboration], CMS-PAS-HIG-16-006.
- [34] G. Aad *et al.* [ATLAS Collaboration], Phys. Rev. Lett. **114**, no. 8, 081802 (2015); G. Aad *et al.* [ATLAS Collaboration], Eur. Phys. J. C **75**, no. 9, 412 (2015); G. Aad *et al.* [ATLAS Collaboration], Phys. Rev. D **92**, 092004 (2015).

- [35] V. Khachatryan *et al.* [CMS Collaboration], Phys. Lett. B **749**, 560 (2015); V. Khachatryan *et al.* [CMS Collaboration], [arXiv:1603.06896 [hep-ex]]; CMS Collaboration [CMS Collaboration], CMS-PAS-HIG-15-013.
- [36] The ATLAS collaboration, ATLAS-CONF-2016-004; The ATLAS collaboration, ATLAS-CONF-2016-017.
- [37] CMS Collaboration [CMS Collaboration], CMS-PAS-HIG-16-002; CMS Collaboration [CMS Collaboration], CMS-PAS-HIG-16-032; CMS Collaboration [CMS Collaboration], CMS-PAS-HIG-17-002.
- [38] CMS Collaboration [CMS Collaboration], CMS-PAS-HIG-16-025.
- [39] The ATLAS collaboration [ATLAS Collaboration], ATLAS-CONF-2016-049.
- [40] M. Frank *et al.*, Phys. Rev. D **94**, no. 5, 055016 (2016).
- [41] The ATLAS Collaboration, ATL-PHYS-PUB-2013-016.
- [42] CMS Collaboration [CMS Collaboration], CMS-PAS-FTR-13-024.
- [43] A. Ahmed *et al.*, arXiv:1512.05771 [hep-ph]; D. Bardhan *et al.*, arXiv:1512.06674 [hep-ph].
- [44] The ATLAS collaboration, ATLAS-CONF-2015-081; CMS Collaboration, CMS-PAS-EXO-15-004.
- [45] M. Toharia, Phys. Rev. D **79**, 015009 (2009).